Study of short and mid-infrared telecom links performance for different climatic conditions

Choé Sauvage [a,b], Clélia Robert [a], Béatrice Sorrente [a], Fréderic Grillot [b], and Didier Erasme [b]

[a] DOTA, ONERA, Université Paris Saclay, 92320 Chatillon - France
[b] LTCI, Télécom Paris, Institut Polytechnique de Paris, 75013 Paris - France

ABSTRACT

This study assesses the performance in term of availability of a FSO (Free Space Optics) link for two wavelengths, belonging to atmospheric windows, the standard telecom wavelength 1.55 μm and the mid-infrared wavelength 4 μm. To do so, we compute the transmission rate under various atmospheric conditions, including fog. Using the atmospheric transmission rate from our radiative transfer software MATISSE, the link budget is derived for a simple direct emission and detection system. The source and detector components characteristics, from commercial data-sheet, are considered to compute the reception noise. An estimate of the Bit Error Rate (BER) of the FSO link for the two wavelengths is presented as a function of visibility. Assuming a bit error correction and the corresponding BER value, it is possible to derive the limit of visibility under which the optical link is cut. A weather visibility database has been collected and compiled for a year to obtain the theoretical availability of the FSO system. As an example the availability at Velizy-Villacoublay (France) weather station throughout the year 2017 is used. In this case the theoretical link availability wins 30 hours of operation in January 2017 with the 4 μm optical wavelength, that shows the benefit of using mid-infrared for FSO when fog occurs.

Keywords: Free Space Optics, Link budget, Infrared transmittance, Scintillation

1. INTRODUCTION

Free Space Optics (FSO) is a growing up technology offering a higher bandwidth with fast and cost-effective deployment compared to fiber technology associated to a lack of regulation unlike radio frequencies [1] and more directivity induced discretion. Multiple applications are envisioned including but not limited to campus-scaled network, substitution for a fiber network after a disaster (e.g., earthquake, attack, etc.) or connecting a drone as a relay in white spot. Despite that, FSO performances are restricted by atmospheric phenomena [2] (e.g., turbulence [3] , fog or scattering [4]). Therefore, the operating wavelength is an important parameter that has to be chosen wisely so as to reduce the impact of the environmental parameters. In order to improve the FSO availability, performance and range, the investigation of the cross relation between the climatic conditions and the wavelength is highly required.

The main scope of this study is to evaluate and compare the performance and the availability of a FSO link of a few kilometers in urban environment for two infrared wavelengths matching the appropriate atmospheric windows [5].

We will compare the standard telecom wavelengths $\lambda = 1.55$ μm and the mid infrared $\lambda = 4$ μm. The wavelength $\lambda = 1.55$ μm is very interesting because it is a well known technology with low cost and dedicated telecom components. It would be very easy to make a transition with the current fiber network. The drawbacks of this wavelength are the hazard of retinal damage, its high level of scintillation in turbulent air and poor transmittance compared to 4 μm [6]. The 4 μm does not show such problems, indeed the use of $\lambda = 4$ μm for a FSO link is very interesting and emerging [7].

This paper is organized as follows: Section 2 presents the system architecture of the FSO link, Section 3 is dedicated to the computing of the link budget of our system. In Section 4 we discuss about the BER performance and the availability of our link, and Section 5 summarizes conclusions and prospects.

For more informations send correspondence to C.Sauvage (chloe.sauvage@onera.fr) or C.Robert (clelia.robert@onera.fr)

2. METHODOLOGY : SYSTEM ARCHITECTURE

To make the comparative study of these two wavelengths, we design a simple and shared optical system. The Figure 1 depicts the optical system, where laser is used as a transmitter. The beam is then enlarged and launched into the atmosphere with a diameter lens $D_E = 10$ cm whose coefficient of transmission is $l_E = 0.95$. The beam crosses the atmosphere on a $Z = 4$ km horizontal path with a $t(\lambda)$ atmospheric transmittance. The flux is collected by an other $D_R = 10$ cm diameter lens of coefficient transmission $l_R = 0.95$, which focuses the beam on the detector.

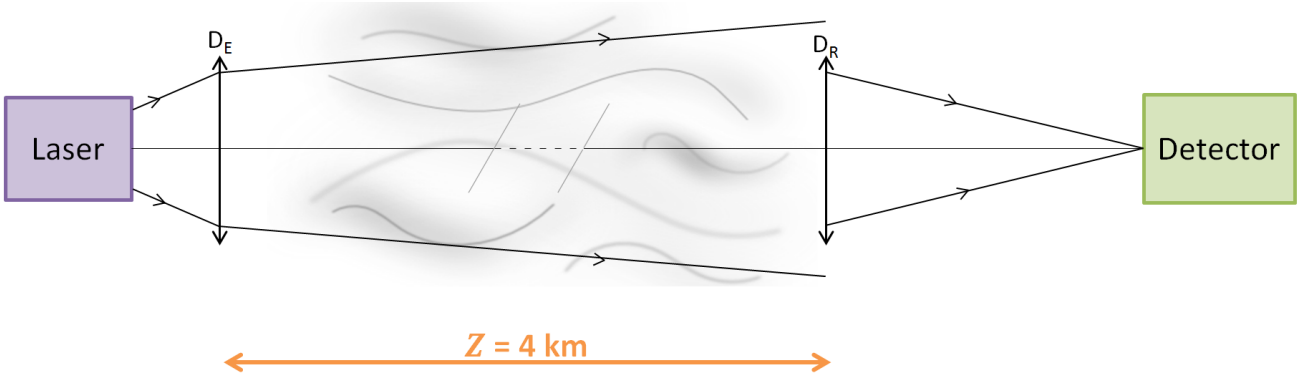

Figure 1. System architecture

The laser light is directly modulated whith an On Off Keying Return to Zero (OOK-RZ) format. The emitted power is 0 mW for bit 0 and 70 mW for bit 1. An emitted power of 70 mW is easily reached by laser diodes and quantum cascade lasers which are found on the market [8]. The binary rate of the modulation is 666 Mbits/s which corresponds to a bandwidth $\Delta f = 532$ MHz. This rate is determined by our signal clock recovery. The characteristics of the laser and the detectors come from commercial components. Their specifications are displayed on Table 1 for both wavelengths.

λ (μm)	1,55	4
R_L (Ω)	50	50
R (A/W)	1	1,3
RIN (dB/Hz)	-120	-150
λ_1 (μm)	0,8	2,5
λ_2 (μm)	1,75	5
θ_M (^{o})	20	18
Area (mm^2)	$\pi \times 0,05^2$	$0,5 \times 0,5$

Table 1. Specifications of components for each wavelength.

3. LINK BUDGET

3.1 Atmospheric transmittance

The first step is to compute the transmittance versus the visibility for the two wavelengths.

For this study, two weather cases are compared with MATISSE [9], our radiative transfer software. The first simulation, on Figure 2a, is made with a winter profile, troposperic aerosols and advection fog. Fog is defined to have a visibility lower or equal to 1 km. The second simulation, on Figure 2b, is similar but without fog. In the two cases which are shown on Figure 2 the transmittance is better at 4 μm than 1.55 μm. These values of transmittance are essential in order to compute the received power for a 4 km path.

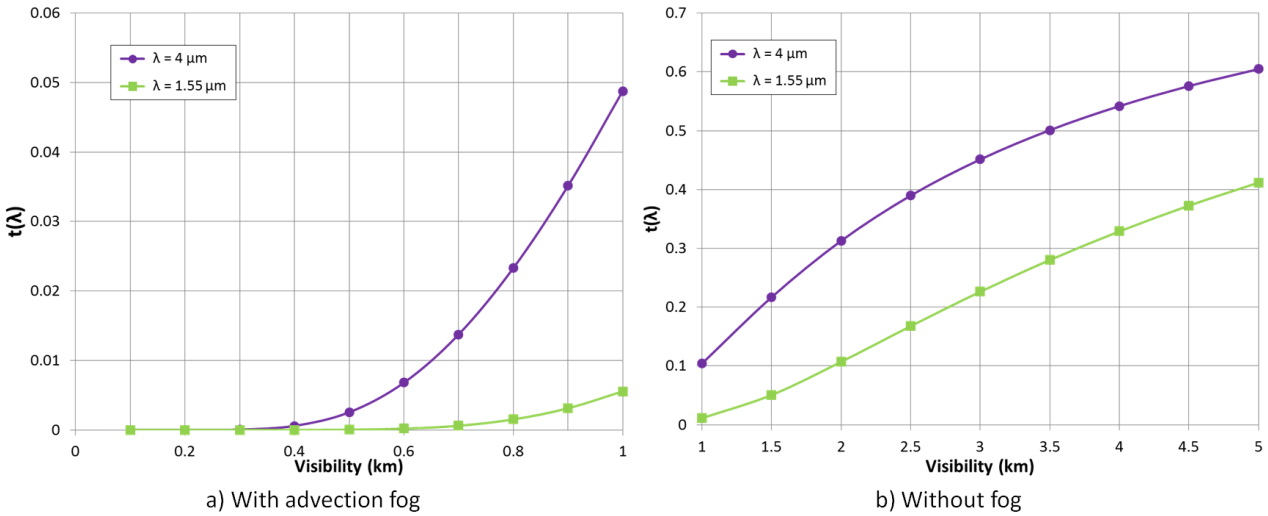

Figure 2. Transmittance as a function of visibility for the two wavelengths. For a winter profile and tropospheric aerosols a) with advection fog b) without fog.

3.2 Received power

The link between the emitted signal flux P_E (in W) and the received signal flux P_R (in W) in case of atmospheric attenuation is given by the Beer-Lambert law:

$$P_R = P_E \; t(\lambda) \; , \tag{1}$$

where Z is the link path (in m) and $t(\lambda)$ the atmospheric transmittance coefficient.

Our system is a non diffracted limited system so the Beer Lambert law follow this equation [10] :

$$P_R = P_E \; \frac{D_R^2}{(D_E + \phi_E Z)^2} t(\lambda) \;\; l_E \; l_R, \tag{2}$$

reminding $D_{E,R}$ (in m) and $l_{E,R}$ are respectively the diameters and lens losses of the transmitter and emitter. We define ϕ_E as the beam divergence angle which is given by $\phi_E = \frac{\lambda}{\pi \omega_0}$ (using the usual truncation equation $\omega_0 = \frac{D_E}{3}$) .

On Figure 3 we compare the evolution of the received power as a function of visibility for an emitted power P_E of 70 mW, which corresponds to bit 1. Figure 3a presents the case with advection fog, showing that $\lambda = 4$ μm is the most powerful link. However Figure 3b, which corresponds to the case without fog, shows that the 4 μm is more interesting in terms of power up to 2.4 km of visibility, whereas beyond, the 1.55 μm wavelength is better. This effect is due to the divergence of the beam and the geometric losses.

4. PERFORMANCE

4.1 Bit Error Rate

The BER enables to assess the performance of a digital communication. For a OKK-RZ modulation, the BER expression is given by [11] :

$$BER = \frac{1}{2} \left[erfc \left(\frac{Q}{\sqrt{2}} \right) \right] \; , \tag{3}$$

with the Q factor following this equation [11] :

$$Q = \frac{I_1 - I_0}{\sigma_1 + \sigma_0} \; . \tag{4}$$

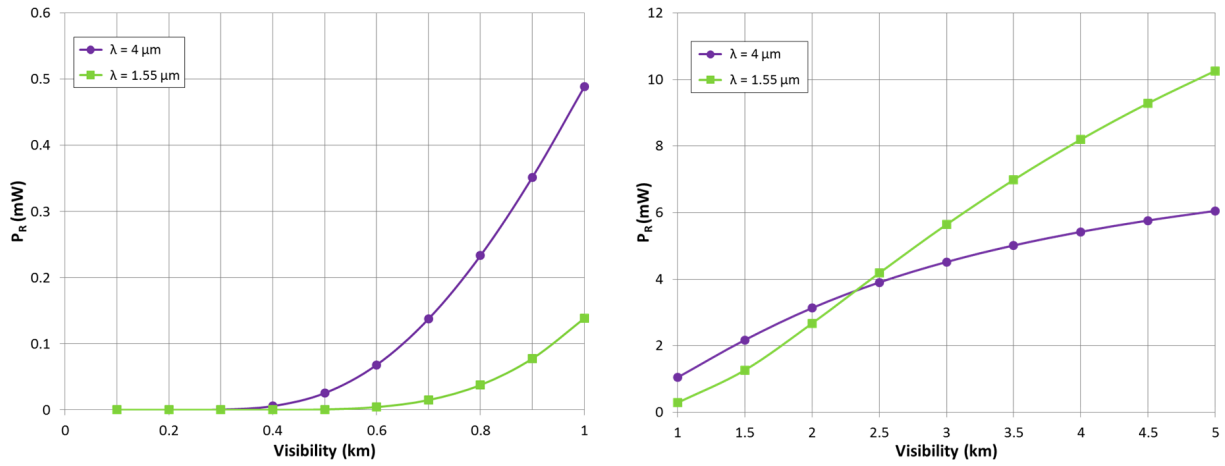

Figure 3. Received power as a function of visibility for the two wavelengths. With an emitted power of 70 mW for a winter profile and tropospheric aerosols a) with advection fog b) without fog.

In Equation (4) $I_{0,1}$ is the photocurrent for the bits $\{0, 1\}$, and $\sigma_{0,1}$ are their respective total noise. When the bit is 0 the photocurrent $I_0 = 0$ and when the bit is 1 the photocurrent $I_1 = I_{max}$. The photocurrent is given by this equation :

$$I = R \cdot P_R \ , \tag{5}$$

with R the responsivity (in A/W) of the detector.

By replacing Q (Equation (4)) in the BER (Equation (3)), it turns to :

$$BER = \frac{1}{2}\left[erfc\left(\frac{1}{\sqrt{2}} \cdot \frac{I_1 - I_0}{\sigma_1 + \sigma_0}\right)\right] \ . \tag{6}$$

In section 3.2 we computed the power received, these values are used in the determination of the BER. Now we can focus on the detection noise of our system, and study its composition.

4.2 Noises

Various noises affect the performance of a telecommunication link. The first one is the shot noise defined by :

$$\sigma_{Sh}^2 = 2eI\Delta f \ , \tag{7}$$

where e is the elementary charge of the electron, I the photocurrent (in A) and Δf the bandwidth (in Hz).

The second noise of the study is the detector thermal noise :

$$\sigma_{Th}^2 = \frac{4kT_{room}}{R_L}\Delta f \ , \tag{8}$$

with k the Boltzmann constant, T_{room} the room temperature (in K), R_L the load resistance (in Ω).

The third noise is the thermal background noise which comes from the thermal radiation of the optics and of the atmosphere. This noise has the following expression :

$$\sigma_{Back}^2 = 2eP_{Back}R\Delta f \ , \tag{9}$$

with P_{Back} (in W) the power of the background which is given by :

$$P_{Back} = S_{Detec}E_{Back} \ , \tag{10}$$

and S_{detec} (E_{Back}) is the detector area (in m^2) (background irradiance (in W/m^2)) .

The total background irradiance is given by :

$$E_{Back} = \pi \sin \theta_D{}^2 \sum_N L_{medium} \ , \tag{11}$$

where θ_D is the field of view of the detector, N the number of crossed medium (atmosphere and lenses) by the beam and L_{medium} the luminance for each medium.

Assuming that each medium produces a black body radiation, the luminance L_{medium} (in $W.m^{-2}.sr^{-1}$) follows this expression :

$$L_{medium} = t'_{medium} \times \int_{\lambda_1}^{\lambda_2} L_{\Omega,\lambda}(\lambda, T_{medium}) d\lambda \ , \tag{12}$$

with t'_{medium} a combination between the emissivity of the regarded medium and the transmission coefficient of crossed path by the background radiation from the emitted medium to the detector. $L_{\Omega,\lambda}(\lambda, T_{medium})$ (in $W.m^{-2}.m^{-1}.sr^{-1}$) is computed by using the Planck law that describes the distribution of the spectral energetic luminance emitted by a black body at the thermodynamic equilibrium for a given temperature. Here T_{medium} is the temperature of the medium for which the background radiation is created. The spectral range of the detector is delimited by the two wavelengths λ_1 and λ_2.

In our system we have $N = 4$ media, they are indexed with their contribution to the luminance in the Table 2 .

Medium	t'_{medium}	T_{medium} (in ^{o}C)
Transmitter lens	$0.05 \times 0.95 \times t(\lambda)$	20
Atmosphere	$0.95 \times t(\lambda)$	10
Received lens	0.05	20
Room	1	20

Table 2. Contribution of each medium in luminance calculation.

The last noise comes from the intensity fluctuations of the laser, named Relative Intensity Noise (RIN). The RIN (dB/Hz) is expressed like in Ref. [12] :

$$RIN = 10 \log \left(\frac{< \delta P(t)^2 >}{P_R^2} \right) - 10 \log(\Delta f) \ , \tag{13}$$

with $< \delta P(t)^2 >$ the temporal square average of intensity fluctuation. So the noise of the laser is :

$$\sigma_{Laser} = R \cdot P_R \sqrt{\Delta f \cdot 10^{RIN/10}} \ , \tag{14}$$

$$\sigma^2_{Laser} = R^2 \cdot P_R^2 \cdot \Delta f \cdot 10^{RIN/10} \ . \tag{15}$$

Finally we sum quadratically the noise variances to obtain the total noise on the detector, so that :

$$\sigma^2_{TOTAL} = \sigma^2_{Sh} + \sigma^2_{Th} + \sigma^2_{Back} + \sigma^2_{Laser} \ . \tag{16}$$

The RIN and the shot noise depend directly of the laser source, contrary to the termal and background noises.

We focus on the scenario with advection fog that is indeed the most restrictive case because of the weakness of atmospheric coefficient transmission. On Figure 4 we investigate the contribution of the noises versus wavelength and visibility. Figure 4a shows the noises contribution for $\lambda = 1.55$ μm. We can observe that the thermal noise dominates until 700 m of visibility and the RIN overlooks after 700 m of visibility. On Figure 4b we focus on noises contribution for $\lambda = 4$ μm, the thermal noise dominates until a visibility close to 1 km, then for a visibility of 1 km the RIN overlooks. The thermal background noise seems to have no variation on both parts of the Figure

4, because of the large scale which use in our case. Between 100 m and 1 km of visibility the variation of this noise is 0.22% for $\lambda = 1.55$ μm and 3.2% for $\lambda = 4$ μm, that is negligible and so not visible.

Moreover we can notice that the total level of noise is very close for $\lambda = 1.55$ μm and $\lambda = 4$ μm up to 800 m of visibility, then the total level noise is higher at $\lambda = 1.55$ μm than at $\lambda = 4$ μm. To study this effect we focus on the evolution of atmospheric transmittance as a function of visibility (Cf. Figure 2a). Indeed from 700 m of visibility $t(\lambda = 1.55\ \mu m)$ increases non linearly, that induces a quadratic increase of $\sigma^2_{Laser}(\lambda = 1.55\ \mu m)$ as a function of visibility. This increase also appers for $t(\lambda = 4\ \mu m)$ from 500 m of visibility. However we can observe on Figure 4b that $\sigma^2_{Laser}(\lambda = 4\ \mu m)$ increases less higher than $\sigma^2_{Laser}(\lambda = 1.55\ \mu m)$, this is due to the fact that the RIN for a $\lambda = 1.55$ μm diode laser is less larger than the RIN for a $\lambda = 4$ μm QCL (Cf. Table 1).

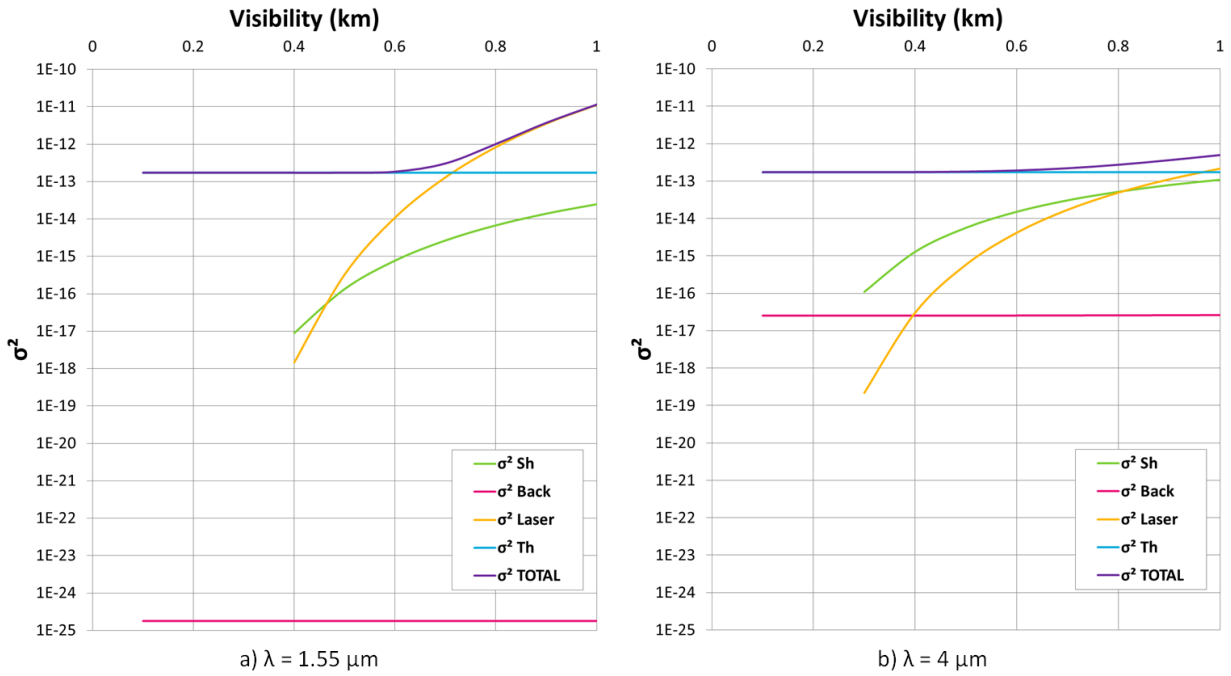

Figure 4. Contribution of noises as a function of visibility for an emitted power of 70 mW and advection fog for a) $\lambda = 1.55$ μm and for b) $\lambda = 4$ μm.

4.3 Yearly availability

We choose to present here the variation of the BER as function of visibility with advection fog (Cf. Figure 5), by using the results previously obtained. The red line on Figure 5 corresponds to a BER limit of 10^{-4}, assuming an error correction code that brings the BER down to a low value of 10^{-9}. This is the limit above which the FSO link is strongly disrupted and does not operate.

Thus, looking at Figure 5, the minimum visibility required to get an effective FSO link is respectively 600 m at 1.55 μm and 300 m at 4 μm. The different values of BER for visibility larger than 900 m for $\lambda = 1.55$ μm and higher than 400 m for $\lambda = 4$ μm, are equal to 0, so they are not plotted.

In order to prepare a future telecom link at ONERA-Chatillon laboratory, we compute a practical availability. We created a weather visibility database which indexes the visibility for each hour at Velizy-Villacoublay (France), a station near our laboratory. The statistics of the database is depicted by the histogram on Figure 6 that represents the visibility variation in 2017. We show in green the visibility lower or equal to 1 km and in blue the visibility larger to 1 km to discriminate fog conditions. On the left part of the graph, we make a focus on low visibility, typical for fog, for the January month. By combining this statistics and the visibility limits it is easy to estimate an availability for each wavelength. Table 3 indexes the theoretical availability for each month and each wavelength.

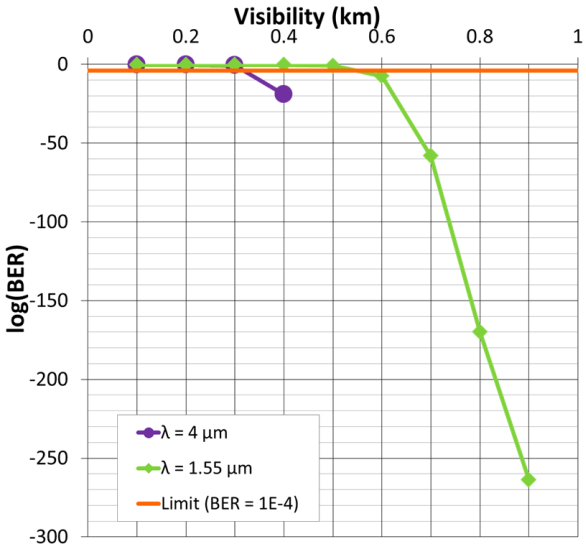

Figure 5. Bit Error Rate versus visibility for two wavelengths and for winter profile with advection fog.

We can observe with the histogram on Figure 6 that in January 2017, fog occurs 15,1 % of the time, so it is an interesting month to make an experiment at low visibility. Hence for January 2017, Table 3 shows that the availability is 87.9 % for the 1.55 μm against 92 % for 4 μm, which represents an increase of 30 hours of operation.

However between April and July, the availability are the same for both wavelengths, but the 4 μm will have an advantage against scintillation : making an experimentation at this period of the year, through hot air could be interesting to lower the impact of the scintillation on the received signal. Indeed the scintillation index σ_I^2 is proportional to $\lambda^{-7/6}$ so scintillation decreases as a function of wavelength.

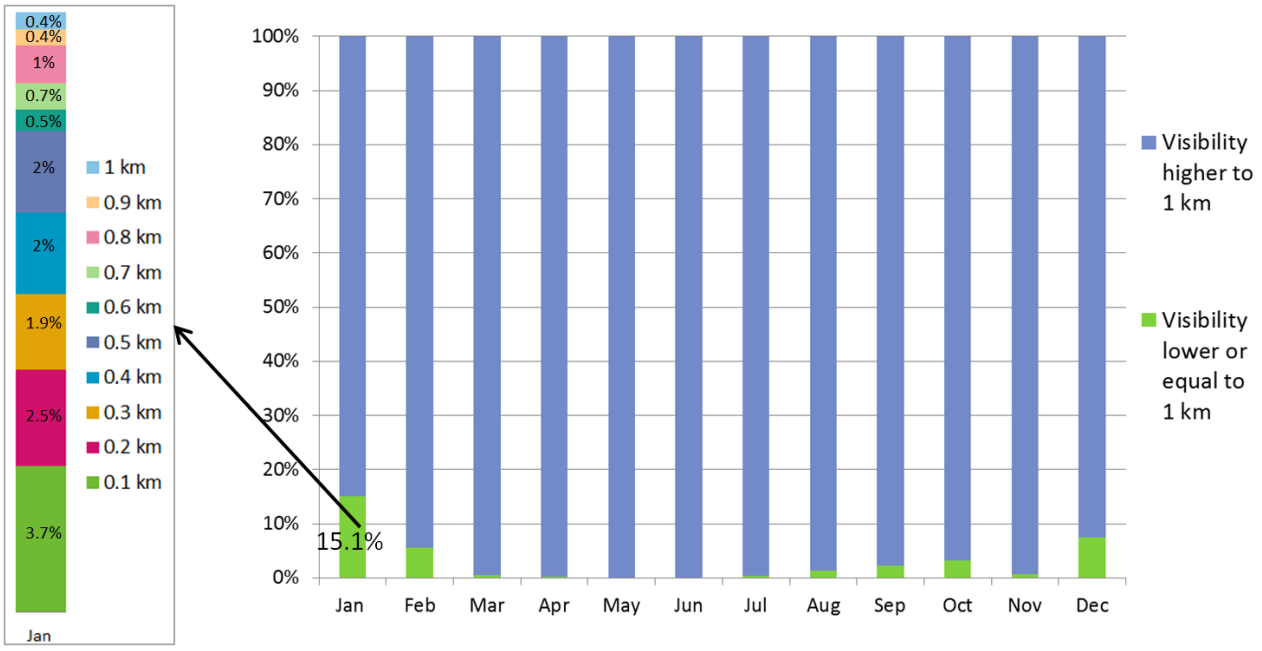

Figure 6. Histogram which depicts the visibility variation in 2017 at Velizy-Villacoublay (France). Focus on visibility $\leq$ 1 km on January (at left).

Mos. / λ	Jan.	Feb.	Mar.	Apr.	May	Jun.	Jul.	Aug.	Sep.	Oct.	Nov.	Dec.	2017
1.55 μm	87.9	95.2	99.7	100	100	100	99.9	98.9	98.3	96.8	99.4	94.4	97.6
4 μm	92.0	96.7	99.9	100	100	100	99.9	99.2	98.9	97.7	99.7	95.3	98.3

Table 3. Availability for each months of 2017 at Velizy-Villacoublay for the two wavelengths.

5. CONCLUSION AND PROSPECTS

The choice of wavelength has an impact on the telecom channel availability especially in the case of fog : the availability of a FSO link will be increased in winter by using a mid-infrared wavelength (4 μm) instead of a short-infrared wavelength (1.55 μm). We saw on this paper that a telecom link at 4 μm wins 30 hours of operation in a foggy month (January 2017 at Velizy-Villacoublay). This result shows the very interesting perspectives of using the mid-infrared wavelength for future FSO links.

In this paper we have presented the transmission simulation on a 4-km horizontal line of sight in a urban environment. We developed a link budget calculation by specifying the received power. Then we described the different detection noises and estimated the BER of our system. Finally we discussed about the availability of our FSO link for the two wavelengths.

This study could be extented to make spatial and temporal (many years) statistics from database assimilation in order to assess on the FSO availability for many conditions (clouds, fog, rain and turbulence).

In the coming months we wish to establish a first FSO link at 4 μm at ONERA-Chatillon, at a bit rate around 600 MHz and for a 4-5 km horizontal path at 40 m height. We plan to do experimentation in winter with low visibility and in summer with strong turbulence. We propose to use our Cn^2 profiler, SCINDAR (SCINtillation Detection And Ranging), working at 4 μm to build this future experiment to get a simultaneously diagnostic of the channel. . The SCINDAR will make the channel diagnostic, by gathering intensity, phase at its telescope aperture and estimating Cn^2 profiles series. This instrument is composed by an infrared Shack-Hartmann wavefront sensor (λ = 3.4 to 4.2 μm) which aims at two halogen lamps 1 m-apart located at several kilometers from the receiver [13]. We have already modified the instrument in order to record the telecom signal on a splitted arm of this bench just before the infrared wavefront sensor. The 4 μm QCL source will be launched by a telescope next to the halogen lamps in a distant building.

REFERENCES

[1] Khalighi, M. A. and Uysal, M., "Survey on Free Space Optical Communication: A Communication Theory Perspective," *IEEE Communications Surveys Tutorials* **16**(4), 2231–2258 (2014).

[2] Sunilkumar, K., Anand, N., Satheesh, S. K., Krishna Moorthy, K., and Ilavazhagan, G., "Performance of free-space optical communication systems: effect of aerosol-induced lower atmospheric warming," *Optics Express* **27**, 11303 (Apr. 2019).

[3] Stotts, L. B., Stadler, B., Hughes, D., Kolodzy, P., Pike, A., Young, D. W., Sluz, J., Juarez, J., Graves, B., Dougherty, D., Douglass, J., and Martin, T., "Optical communications in atmospheric turbulence," **7464**, 746403, International Society for Optics and Photonics (Aug. 2009).

[4] Esmail, M. A., Fathallah, H., and Alouini, M. S., "Outdoor FSO Communications Under Fog: Attenuation Modeling and Performance Evaluation," *IEEE Photonics Journal* **8**, 1–22 (Aug. 2016).

[5] Wallace, J. M. and Hobbs, P. V., [*Atmospheric Science - An Introductory Survey*], Elsevier, second edition ed. (2006).

[6] Ghassemlooy, Z. and Popoola, W. O., "Terrestrial Free-Space Optical Communications," *Mobile and Wireless Communications Network Layer and Circuit Level Design* (2010).

[7] Delga, A. and Leviandier, L., "Free-space optical communications with quantum cascade lasers," in [*Quantum Sensing and Nano Electronics and Photonics XVI*], **10926**, 1092617, International Society for Optics and Photonics (Feb. 2019).

[8] Patel, C. K. N., "High power infrared QCLs: advances and applications," in [*Quantum Sensing and Nanophotonic Devices IX*], **8268**, 826802, International Society for Optics and Photonics (Jan. 2012).

[9] "MATISSE-V3.0 | Matisse." https://matisse.onera.fr/en.

[10] El-Wakeel, A. S., Mohammed, N. A., and Aly, M. H., "Free space optical communications system performance under atmospheric scattering and turbulence for 850 and 1550 nm operation," *Applied Optics* **55**, 7276–7286 (Sept. 2016).

[11] Agrawal, G. P., [*Fiber-Optic Communication Systems*], John Wiley & Sons (Feb. 2012).

[12] Hashemi, S. E., "Relative Intensity Noise (RIN) in High-Speed VCSELs for Short Reach Communication," (2012).

[13] Nguyen, K.-L., Robert, C., Cohard, J. M., Lagouarde, J.-P., Irvine, M., Conan, J.-M., and Mugnier, L. M., "Measurement of the spatial distribution of atmospheric turbulence with SCINDAR on a mosaic of urban surfaces," **10425**, 104250L, International Society for Optics and Photonics (Oct. 2017).